Power Electronics and Drives
Volume 9(44), 2024 DOI: 10.2478/pead-2024-0005

sciendo

Power Electronics and Drives

Novel Speed Sensorless DTC Design for a Five-Phase Induction Motor with an Intelligent Fractional Order Controller Based-MRAS Estimator

Research paper

Sifelislam Guedida[1,*], Bekheira Tabbache[1], Khaled Mohammed Said Benzaoui[2], Kamal Nounou[1], Mokhtar Nesri[3]

[1]*UER ELT, Ecole Militaire Polytechnique, 16111 Algiers, Algeria*
[2]*Faculté des Sciences Appliquées, Laboratoire LAGE Univ Ouargla, Ouargla 30 000, Algeria*
[3]*École Supérieure Ali Chabati, Algiers, Algeria*

Received: 21 November, 2023; Accepted: 15 January 2024

Abstract: This paper presents a fractional-order adaptive mechanism-based model reference adaptive system (MRAS) configuration for speed estimation of sensorless direct torque control (DTC) of a five-phase induction motor. In effect, the fractional-order proportional-integral (FOPI) controller parameters are obtained by the particle swarm optimisation (PSO) algorithm to enhance the MRAS observer response. Thus, the developed algorithm in the speed loop control of the DTC strategy to increase its robustness against disturbances. Moreover, a comparative study has been done of the proposed MRAS-PSO/FOPI speed estimator with the conventional MRAS-proportional-integral (PI) and the PSO-based MRAS-PI. Simulation results have carried out of the different controllers used in the adaptation mechanism of the MRAS estimator, to show the performance and robustness of the proposed MRAS-PSO/FOPI algorithm in use.

Keywords: *sensorless speed • PSO algorithm • model reference adaptive system • direct torque control • fractional-order proportional-integral controller*

1. Introduction

Recently, multiphase machines have attracted the attention of many researchers due to their numerous advantages compared with conventional three-phase machines (Bermudez et al., 2018; Rigatos et al., 2023). Several multiphase machine topologies, such as five-phase (Pavithran et al., 1988; Reddy and Devabhaktuni, 2022), six-phase (González-Prieto et al., 2019a), seven-phase (Yang et al., 2021), nine-phase (González-Prieto et al., 2019) and fifteen-phase (Slunjski et al., 2020) machines, have presented low torque pulsation, high electrical system reliability and improved fault tolerance capability. Hence, multiphase machines cover an extensive power range, enabling them to be used in various fields such as electric aircraft, naval propulsion, electric and hybrid vehicles and high-power industrial applications (Levi, 2008; Salem and Narimani, 2019). In terms of control, many techniques of methods have been developed for simple three-phase machines, such as field-oriented control (FOC) (Zellouma et al., 2023), predictive control (Stando and Kazmierkowski, 2020) and the backstepping technique (Saad et al., 2019), which can be extended to multiphase induction machines by further exploiting the additional degrees of freedom of multiphase machines (Liu et al., 2018). These techniques offer good dynamic performance.

* *Email: d_guedida.sifelislam@emp.mdn.dz*

However, the major drawback of these control techniques is their sensitivity to variations in the machine parameters (Wang et al., 2018). Therefore, direct torque control (DTC) can effectively overcome these drawbacks, particularly with FOC. Recently, DTC for multiphase machines has attracted the attention of researchers due to its simplicity, fast response and robustness (Duran et al., 2017; Guedida et al., 2023). In this context, this paper deals with an adaptive DTC of five-phase induction motor to benefit from the advantages of the control approach and multiphase topologies.

Recently, many sensorless DTC techniques of three-phase machines have been developed to reduce the cost and increase the reliability of electric drive systems in specific applications (El Ouanjli et al., 2022). For this, motor speed can be obtained by models using measured inputs (voltage and current) (Bahloul et al., 2019; Boztas and Aydogmus, 2022; Han and Zhang, 2019; Holakooie et al., 2018; Krim and Mimouni, 2023). In this context, several methods have been proposed in the literature, such as the adaptive Luenberger observer (LO) (Yousfi et al., 2022), the extended Kalman filter (EKF) (Boztas and Aydogmus, 2022) and the full-order sliding mode observer (Zhou et al., 2021), to ensure sensorless control of the simple three-phase motor. Hence, a model-reference adaptive system (MRAS) is widely used in sensorless control of industrial applications (Astrom, 1996). However, due to the lack of efficient tuning criteria, the MRAS speed estimator becomes imprecise. In this objective, many optimisation algorithms can be adopted to improve the efficiency of the classical Proportional-Integral-Derivative (PID) such as the genetic algorithm (GA) (Sahraoui et al., 2017), artificial bee colony method (ABC) (Szczepanski et al., 2019), whale optimisation algorithm (WOA) and improved (IWOA) (Gharehchopogh and Gholizadeh, 2019), particle swarm optimisation (PSO) (Abd Samat et al., 2016), and the methods of S. Ekinci, B. Hekimoğlu and D. Izci (Ekinci et al., 2021), M. Khalilpuor, N. Razmjooy, H. Hosseini and P. Moallem (Khalilpour et al., 2011), J. Agarwal, G. Parmar, R. Gupta and A. Sikander (Agarwal et al., 2018). For this, this paper presents a new approach to speed estimation for the five-phase induction machine drive using an MRAS based on the PSO algorithm. It consists of optimising the parameters of the classical proportional-integral (PI) controller of the MRAS and therefore improving the overall system performance. So, the proposed sensorless DTC scheme combines the PSO algorithm of the classical PI controller parameters in the speed regulator loop to offer noise attenuation and disturbance rejection performance. Moreover, fractional order theory is also introduced in the developed sensorless control of a five-phase induction motor. A fractional-order proportional-integral (FOPI) controller can guarantee accurate speed estimation (He et al., 2021). An FOPI controller is a structure based on the theory of fractional calculus (FC), which has the advantage of a supplementary degree of freedom compared with the classical PI controller (Das et al., 2013; Razzaghian et al., 2022; Zhang et al., 2020). This technique aims to improve the performance of the MRAS of DTC for the five-phase induction motor. For this, two FOPI controllers, are used to replace the classical PI controllers of the adaptation mechanism and the speed loop control. In this paper, the PSO algorithm is employed to provide optimal values of the gains of the FOPI controllers.

In this context, this paper is structured as follows: (1) a mathematical model of the five-phase induction motor, followed by a brief discussion of the DTC principle, (2) an analytical study of the conventional MRAS and the development of the estimator based on the PSO algorithm, (3) design of the adaptive estimator using the intelligent fractional order controller and (4) simulations to confirm the validity and effectiveness of the proposed control.

2. DTC of Five-Phase Induction Motor

2.1. Five-phase induction motor mathematical model

Figure 1 shows a drive system based on a five-phase induction motor powered by a two-level five-phase voltage source inverter (VSI). The stator windings are symmetrically distributed, with a fixed spatial shift of $\vartheta = 2\ \pi/5$ between two consecutive phases (Bermudez et al., 2018). The five-phase induction motor model can be presented with the inverter equations related to the switching states for each power leg (Martin et al., 2017). The vector $[S_a\ S_b\ S_c\ S_d\ S_e]$ can identify 32 switching states, generating 32 voltage vectors containing 30 non-zero vectors and 2 zero vectors (Bermudez et al., 2018). Moreover, according to Eqs (1) and (2), the voltage vectors can

be projected into two orthogonal stationary subspaces (α–β) and (x–y), as shown in Figure 2 (Bermudez et al., 2018).

$$\begin{bmatrix} V_{sa} \\ V_{sb} \\ V_{sc} \\ V_{sd} \\ V_{se} \end{bmatrix} = \frac{V_{dc}}{5} \begin{bmatrix} 4 & -1 & -1 & -1 & -1 \\ -1 & 4 & -1 & -1 & -1 \\ -1 & -1 & 4 & -1 & -1 \\ -1 & -1 & -1 & 4 & -1 \\ -1 & -1 & -1 & -1 & 4 \end{bmatrix} \begin{bmatrix} S_a \\ S_b \\ S_c \\ S_d \\ S_e \end{bmatrix} \quad (1)$$

$$\begin{bmatrix} V_{s\alpha} \\ V_{s\beta} \\ V_{sx} \\ V_{sy} \\ V_{sz} \end{bmatrix} = \frac{2}{5} \begin{bmatrix} 1 & cos\vartheta & cos2\vartheta & cos3\vartheta & cos4\vartheta \\ 0 & sin\vartheta & sin2\vartheta & sin3\vartheta & sin4\vartheta \\ 1 & cos2\vartheta & cos4\vartheta & cos\vartheta & cos3\vartheta \\ 0 & sin2\vartheta & sin4\vartheta & sin\vartheta & sin3\vartheta \\ \frac{1}{2} & \frac{1}{2} & \frac{1}{2} & \frac{1}{2} & \frac{1}{2} \end{bmatrix} \begin{bmatrix} V_{sa} \\ V_{sb} \\ V_{sc} \\ V_{sd} \\ V_{se} \end{bmatrix} \quad (2)$$

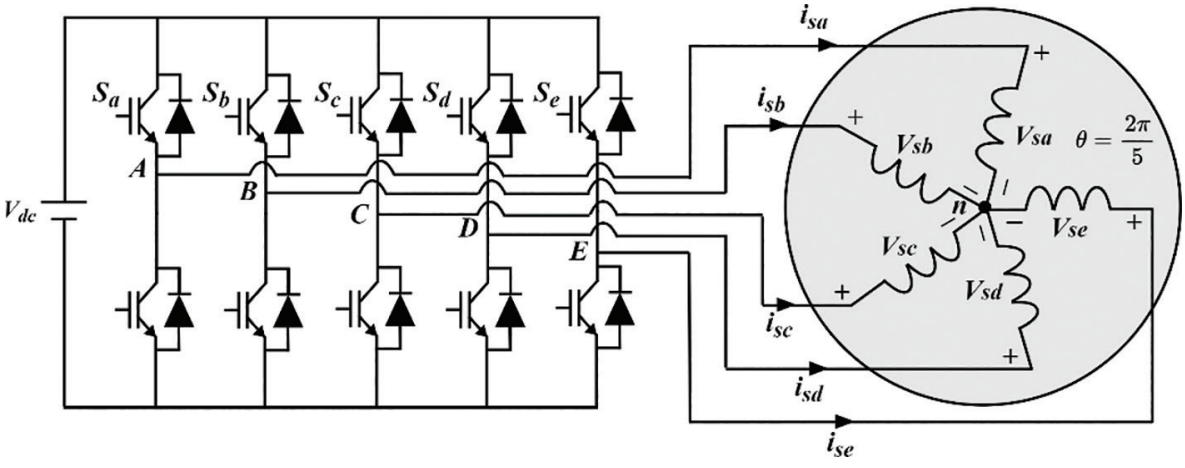

Fig. 1. Five-phase induction motor drive scheme.

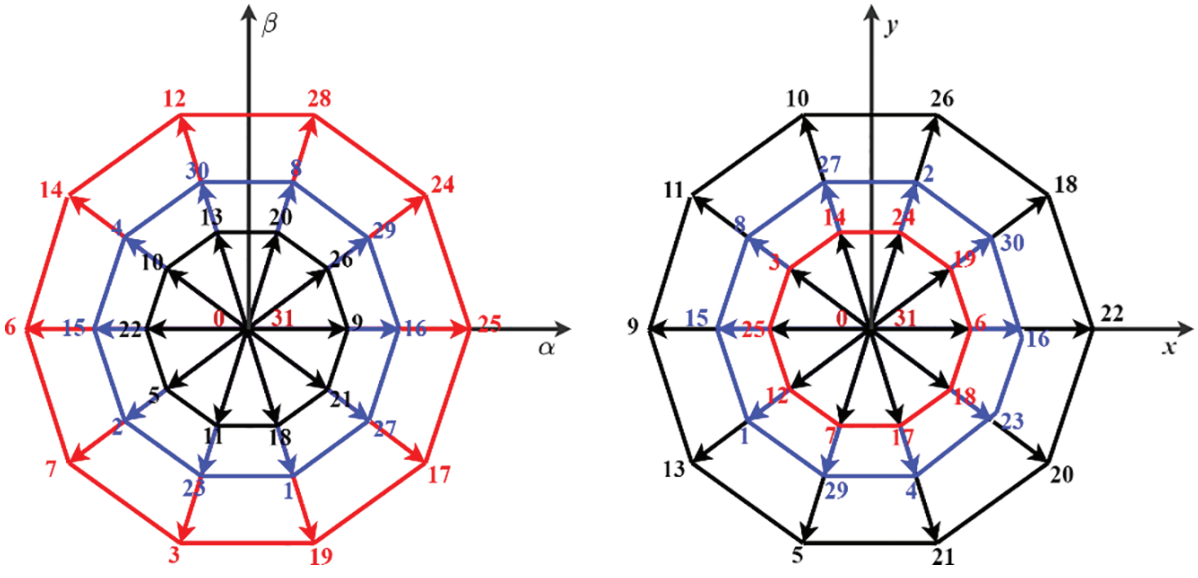

Fig. 2. Voltage space vectors of the five-phase inverter: left side-(α–β subspace) and right side-(x–y subspace).

A five-phase induction motor can be modelled using voltage and flux equations obtained from the electrical and magnetic circuits of the stator and rotor windings (Bermudez et al., 2018). Therefore, it is necessary to consider specific simplifying hypotheses, such as sinusoidal magnetomotive force (MMF) distribution, uniform air gap length, a symmetrical non-saturated armature, negligible core losses (hysteresis and eddy currents are negligible) and identical windings for all phases of the machine (Bermudez et al., 2018). According to these hypotheses, the model of the five-phase induction motor can be written as the following equations (Bermudez et al., 2018):

$$\begin{cases} V_{s\alpha} = R_s I_{s\alpha} + \dfrac{\partial}{\partial t}\phi_{s\alpha} \\ V_{s\beta} = R_s I_{s\beta} + \dfrac{\partial}{\partial t}\phi_{s\beta} \\ V_{sx} = R_s I_{sx} + \dfrac{\partial}{\partial t}\phi_{sx} \\ V_{sy} = R_s I_{sy} + \dfrac{\partial}{\partial t}\phi_{sy} \\ V_{sz} = R_s I_{sz} + \dfrac{\partial}{\partial t}\phi_{sz} \end{cases} \tag{3}$$

$$\begin{cases} V_{r\alpha} = R_r I_{r\alpha} + \omega\phi_{r\beta} + \dfrac{\partial}{\partial t}\phi_{r\alpha} \\ V_{r\beta} = R_r I_{r\beta} - \omega\phi_{r\alpha} + \dfrac{\partial}{\partial t}\phi_{r\beta} \\ V_{rx} = R_r I_{rx} + \dfrac{\partial}{\partial t}\phi_{rx} \\ V_{ry} = R_r I_{ry} + \dfrac{\partial}{\partial t}\phi_{ry} \\ V_{rz} = R_r I_{rz} + \dfrac{\partial}{\partial t}\phi_{rz} \end{cases} \tag{4}$$

$$\begin{cases} \phi_{s\alpha} = (L_{ls} + L_m) I_{s\alpha} + L_m I_{r\alpha} \\ \phi_{s\beta} = (L_{ls} + L_m) I_{s\beta} + L_m I_{r\beta} \\ \phi_{sx} = L_{ls} I_{sx} \\ \phi_{sy} = L_{ls} I_{sy} \\ \phi_{sz} = L_{ls} I_{sz} \end{cases} \tag{5}$$

$$\begin{cases} \phi_{r\alpha} = (L_{lr} + L_m) I_{r\alpha} + L_m I_{s\alpha} \\ \phi_{r\beta} = (L_{lr} + L_m) I_{r\beta} + L_m I_{s\beta} \\ \phi_{rx} = L_{lr} I_{rx} \\ \phi_{ry} = L_{lr} I_{ry} \\ \phi_{rz} = L_{lr} I_{rz} \end{cases} \tag{6}$$

The electromagnetic torque of a five-phase induction motor can be expressed as:

$$T_e = P L_m (I_{r\alpha} I_{s\beta} - I_{s\alpha} \mathrm{I}_{s\beta}) \tag{7}$$

where R_s and L_{ls} are the resistance and leakage inductance of the stator.

R_r and L_{ls} are the resistance and leakage inductance of the rotor.

$V_{s\alpha}$, $V_{s\beta}$, V_{sx}, V_{sy} and V_{sz} are the stator voltage in the α, β, x, y and z axes.

$V_{r\alpha}$, $V_{r\beta}$, V_{rx}, V_{ry} and V_{rz} are the rotor voltage in the α, β, x, y and z axes.

$\phi_{s\alpha}$, $\phi_{s\beta}$, ϕ_{sx}, ϕ_{sy} and ϕ_{sz} are the stator flux in the α, β, x, y and z axes.

$\phi_{r\alpha}$, $\phi_{r\beta}$, ϕ_{rx}, ϕ_{ry} and ϕ_{rz} are the rotor flux in the α, β, x, y and z axes.

$I_{s\alpha}$, $I_{s\beta}$, I_{sx}, I_{sy} and I_{sz} are the stator current in the α, β, x, y and z axes.
$I_{r\alpha}$, $I_{r\beta}$, I_{rx}, I_{ry} and I_{rz} are the rotor current in the α, β, x, y and z axes.
L_m is the magnetising inductance, ω is rotor angular speed and P is the number of pole pairs.
T_e is the electromagnetic torque.

It is necessary to note that the stator and rotor components related to the axes (α–β) contribute to an electromagnetic torque similar to that of a simple three-phase machine, as shown in Eq. (7). Furthermore, according to Eqs (3)–(6), it is clear that the (x–y) subspace can generate significant circulation currents in the five-phase induction machine. Moreover, zero sequence components are neglected due to the short-circuited rotor winding and the balanced star connection of the five-phase stator windings.

2.2. DTC scheme of five-phase induction machine

The approach of DTC has been recognised as a robust control strategy to ensure a fast dynamic response of induction motor. Therefore, the study of DTC for the five-phase induction machine is similar to that of DTC for a three-phase motor, with a modified switching table, as shown in Figure 3. The high number of generated voltage vectors (32) in the (α–β) subspace allows an increase in the number of sectors (10 sectors), as illustrated in Figure 2. In this paper, DTC based on large voltage vectors are opted for five-phase motors to ensure a fast torque response and minimise voltage vectors in the (x–y) subspace (Bermudez et al., 2018; Kim and Kim, 2009).

Figure 4 shows that the 10 large voltage vectors can divide the subspace (α–β) into 10 sectors (k = I, II, …, X). Table 1 shows the selected voltage vector using the output error of the regulators (stator flux and torque hysteresis regulators) and the sector in which the stator flux is located. For more clarity, the voltage vector chosen by the switching table can increase or decrease the magnitude of stator flux and electromagnetic torque for each sampling period.

3. Speed Sensorless DTC Scheme Based on MRAS Estimator

3.1. Conventional MRAS estimator

In high-power industrial applications, motor speed feedback information is essential. The mechanical speed sensor is a crucial tool to provide this information. However, this sensor is easily disturbed by mechanical noise, its maintenance is costly and its reliability is reduced. Therefore, recent research has focused on developing sensorless controls for electric drives to eliminate mechanical tools. The MRAS approach was found to be an alternative technique for ensuring speed estimation in the drive of three-phase induction motors. Therefore, Figure 5 shows the DTC associated with an MRAS for the five-phase induction machine (DTC-MRAS-PI).

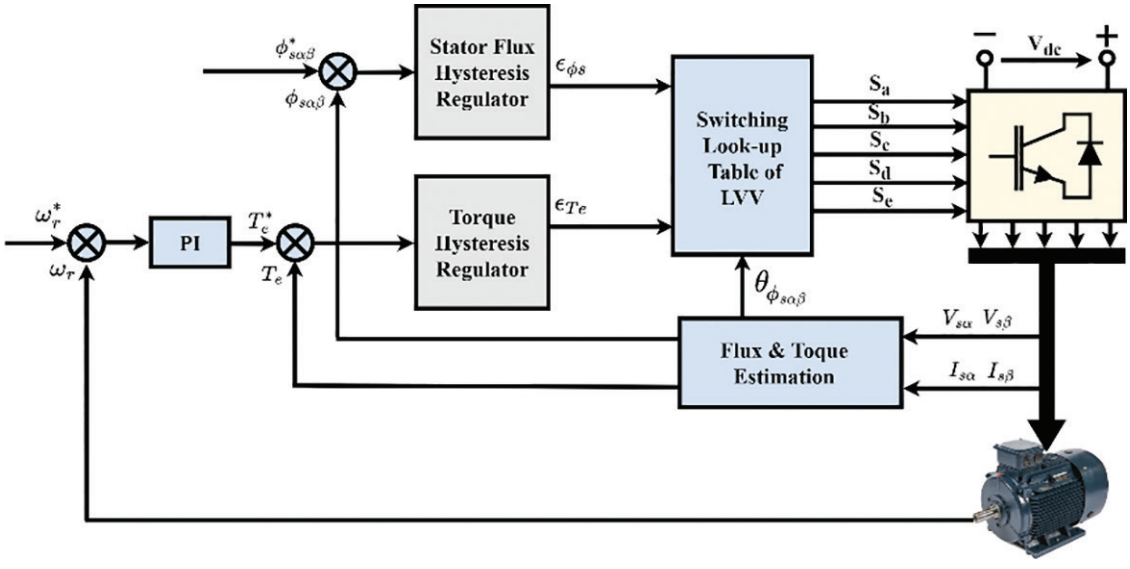

Fig. 3. Principle of DTC of the five-phase induction machine. DTC, direct torque control; PI, proportional-integral.

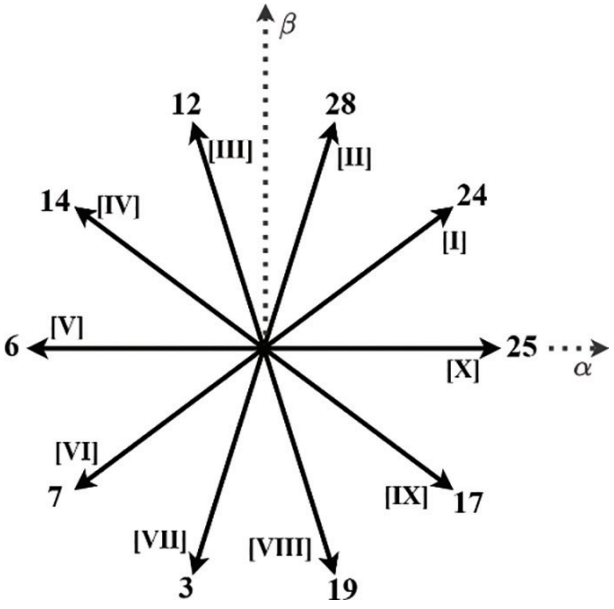

Fig. 4. Voltage vectors and sectors in subspace (α–β).

Sector k	I	II	III	IV	V	VI	VII	VIII	IX	X
$\epsilon_{\phi s}=1,\epsilon_{Te}=1$	28 [11100]	12 [01100]	14 [01110]	6 [00110]	7 [00111]	3 [00011]	19 [10011]	17 [10001]	25 [11001]	24 [11000]
$\epsilon_{\phi s}=-1,\epsilon_{Te}=1$	12 [01100]	14 [01110]	6 [00110]	7 [00111]	3 [00011]	19 [10011]	17 [10001]	25 [11001]	24 [11000]	28 [11100]
$\epsilon_{\phi s}=1,\epsilon_{Te}=-1$	19 [10011]	17 [10001]	25 [11001]	24 [11000]	28 [11100]	12 [01100]	14 [01110]	6 [00110]	7 [00111]	3 [00011]
$\epsilon_{\phi s}=-1,\epsilon_{Te}=-1$	3 [00011]	19 [10011]	17 [10001]	25 [11001]	24 [11000]	28 [11100]	12 [01100]	14 [01110]	6 [00110]	7 [00111]
$\epsilon_{\phi s}=1,\epsilon_{Te}=0$	0 [00000]	31 [11111]	0 [00000]	31 [11111]	0 [00000]	31 [11111]	0 [00000]	31 [11111]	0 [00000]	31 [11111]
$\epsilon_{\phi s}=-1,\epsilon_{Te}=0$	0 [00000]	31 [11111]	0 [00000]	31 [11111]	0 [00000]	31 [11111]	0 [00000]	31 [11111]	0 [00000]	31 [11111]

DTC, direct torque control.
where $\epsilon_{\phi s}$ is the control output of the flux hysteresis controller.
ϵ_{Te} is the control output of the torque hysteresis controller.

Table 1. Switching table for DTC (with reference to Figure 4 when $\phi_{s\alpha\beta}$ is in Sector k).

Figure 6 shows a block diagram of the MRAS speed estimator for the five-phase induction machine. The adaptation process is developed by the rotor flux and stator voltage equations projected into the (α–β) subspace. It is clear that the technique is based on two decoupled models of the five-phase induction motor to ensure the desired estimation. The reference model (voltage model) requires only measured stator currents and voltages and does not depend on rotor speed information. However, the second adaptive model (current model) requires the estimated rotor speed information and the measured stator current to adjust the rotor flux output. In this section, the error defined between the output of the reference model and the output of the adaptive model has been generated by an adaptation mechanism based on the classical PI controller with manual gain adjustment. According to the machine equations in the stationary reference frame (α–β), the two models can be written as follows.

- **Reference Model (Voltage Model):**

$$\begin{cases} \dfrac{d\hat{\phi}_{r\alpha V}}{dt}=\dfrac{L_r}{L_m}\left(V_{s\alpha}-R_sI_{s\alpha}-\sigma L_s\dfrac{dI_{s\alpha}}{dt}\right) \\ \dfrac{d\hat{\phi}_{r\beta V}}{dt}=\dfrac{L_r}{L_m}\left(V_{s\beta}-R_sI_{s\beta}-\sigma L_s\dfrac{dI_{s\beta}}{dt}\right) \end{cases} \quad (8)$$

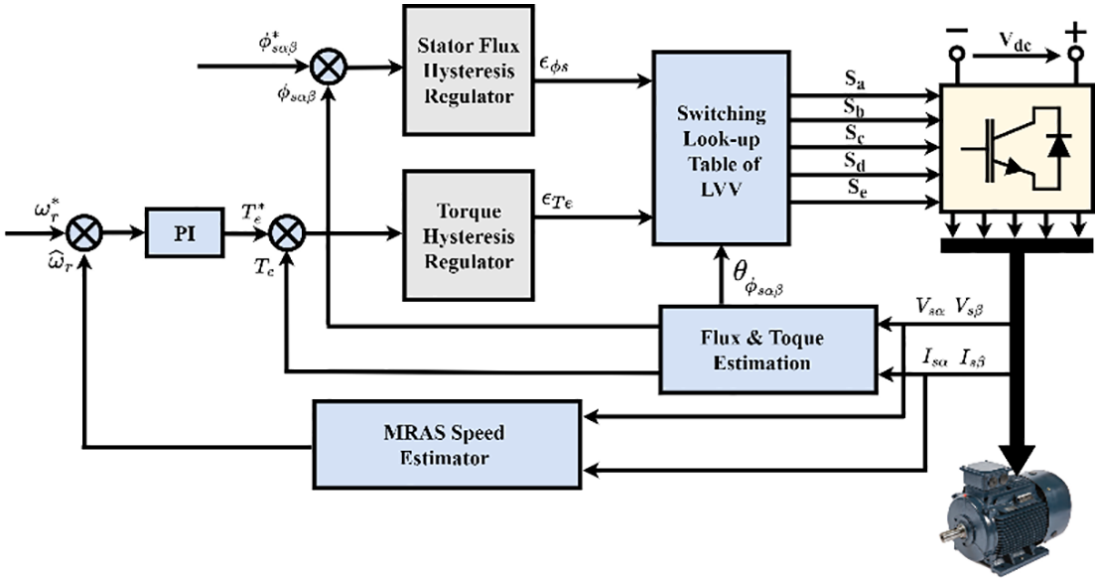

Fig. 5. Block diagram of speed sensorless control (conventional DTC-MRAS-PI) of five-phase induction motor. DTC, direct torque control; MRAS, model reference adaptive system; PI, proportional-integral.

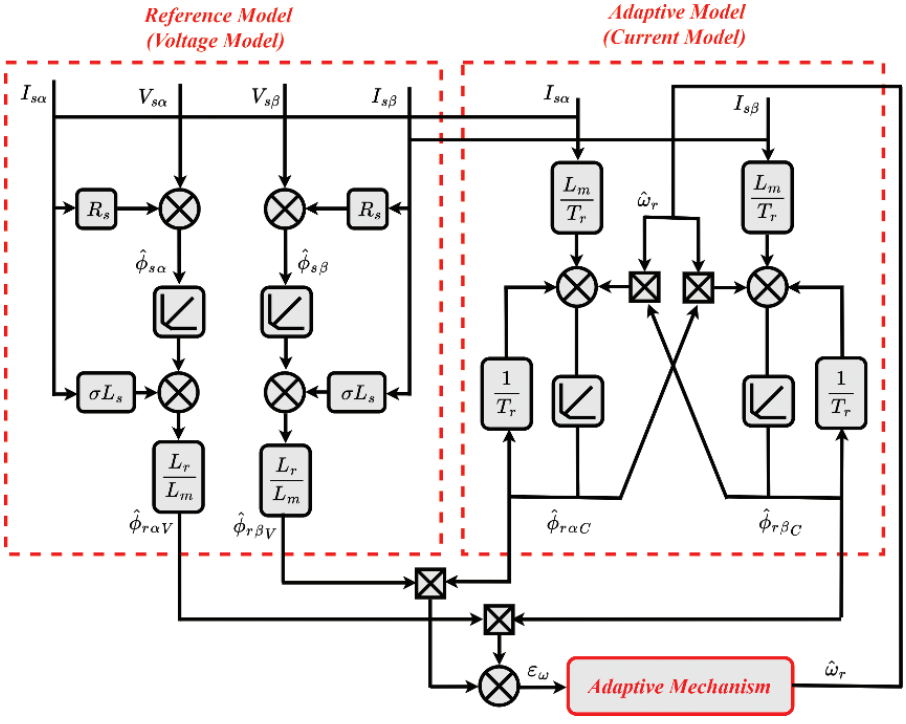

Fig. 6. Block diagram of model adaptive reference system (MRAS) based on rotor flux. MRAS, model reference adaptive system.

- **Adaptive Model (Current Model):**

$$\begin{cases} \dfrac{d\hat{\phi}_{r\alpha C}}{dt} = \dfrac{R_r L_m}{L_r} I_{s\alpha} - \dfrac{R_r}{L_r}\hat{\phi}_{r\alpha C} + \hat{\omega}_r \hat{\phi}_{r\beta C} \\ \dfrac{d\hat{\phi}_{r\beta C}}{dt} = \dfrac{R_r L_m}{L_r} I_{s\beta} - \dfrac{R_r}{L_r}\hat{\phi}_{r\beta C} + \hat{\omega}_r \hat{\phi}_{r\alpha C} \end{cases} \quad (9)$$

$$\begin{cases} \dfrac{d\hat{\phi}_{r\alpha C}}{dt} = \dfrac{L_m}{T_r} I_{s\alpha} - \dfrac{1}{T_r}\hat{\phi}_{r\alpha C} + \hat{\omega}_r \hat{\phi}_{r\beta C} \\ \dfrac{d\hat{\phi}_{r\beta C}}{dt} = \dfrac{L_m}{T_r} I_{s\beta} - \dfrac{1}{T_r}\hat{\phi}_{r\beta C} + \hat{\omega}_r \hat{\phi}_{r\alpha C} \end{cases} \tag{10}$$

where $\sigma = 1 - \dfrac{L_m^2}{L_s L_r}$, $T_r = \dfrac{L_r}{R_r}$ are the leakage coefficient and the rotor time constant, respectively.

$\hat{\phi}_{r\alpha C}$ is the rotor flux of the α component in the current model.
$\hat{\phi}_{r\beta C}$ is the rotor flux of the β component in the current model.
$\hat{\phi}_{r\alpha V}$ is the rotor flux of the α component in the voltage model.
$\hat{\phi}_{r\beta V}$ is the rotor flux of the β component in the voltage model.
$\hat{\omega}_r$ is the estimated speed.

The error between the output of the reference model and the output of the adaptive model is defined by the following equation:

$$\varepsilon_\omega = \hat{\phi}_{r\alpha C}\hat{\phi}_{r\beta V} - \hat{\phi}_{r\beta C}\hat{\phi}_{r\alpha V} \tag{11}$$

where ε_ω is the error quantity for the speed estimation.

To ensure the stability of the estimated speed, a classical PI controller can be used to define an adaptation law presented in Eq. (12) based on the error input of the estimated rotor fluxes and Popov's hyperstability theorem (Schauder, 1989).

$$\hat{\omega}_r = \left(k_p + \frac{k_i}{s}\right)\varepsilon_\omega \tag{12}$$

3.2. Proposed MRAS speed estimator based on PSO algorithm

PSO is a population-based metaheuristic technique used to solve optimisation problems. It simulates the social behaviour of birds flying in groups to reach their food source. This social–psychological behaviour inspired Russell Eberhart and James Kennedy (Kennedy and Eberhart, 1997) to apply this principle to problem-solving. In recent years, PSO has attracted considerable interest due to its simple process, its easy implementation in a variety of fields and its remarkable effectiveness in solving complex optimisation problems. Velocity control in the PSO algorithm is the main element used to determine the direction and position of a swarm of particles in order to search for an optimal solution in the search space. The design of this control approach is based on inertia coefficients, which are presented in Eqs (13) and (14) to facilitate the algorithm's convergence towards an optimal solution. Figure 7 shows a typical geometrical demonstration to justify the stability of a particle's movement in the PSO process. For the principle to be respected, the particles in the swarm must not move randomly but need better information from the best global particle:

$$V_i(k+1) = w * V_i(k) + C_1 * r_1\left[P_i(k) - x_i(k)\right] + C_2 * r_2\left[G_i(k) - x_i(k)\right] \tag{13}$$

$$x_i(k+1) = x_i(k) + V_i(k+1) \tag{14}$$

where w is the coefficient of inertia.

C_1 and C_2 are the coefficients of acceleration.

r_1 and r_2 are two random numbers drawn uniformly in [0,1] at each iteration and for each dimension.

$V_i(k)$ is the velocity of the particles at iteration k.

$x_i(k)$ is the current position of the particles in the search space.

In the MRAS estimator for the five-phase induction machine using in the speed sensorless DTC, the adaptation mechanism is realised by a classical PI controller. It is important to note that if the controller parameters are not optimal, the MRAS speed estimator can be disturbed by parametric variations in the system drive. Furthermore, this disturbance can lead to poor speed estimation in the five-phase induction machine. To increase the robustness of sensorless DTC for the five-phase induction machine, a PSO algorithm will be used to optimise the classical

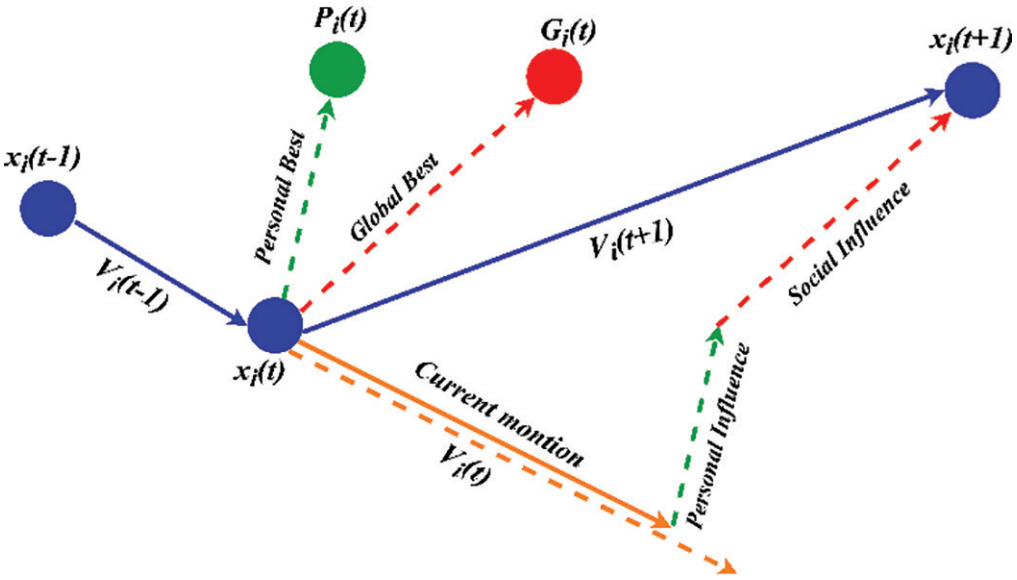

Fig. 7. Movement of the PSO swarm. PSO, particle swarm optimisation.

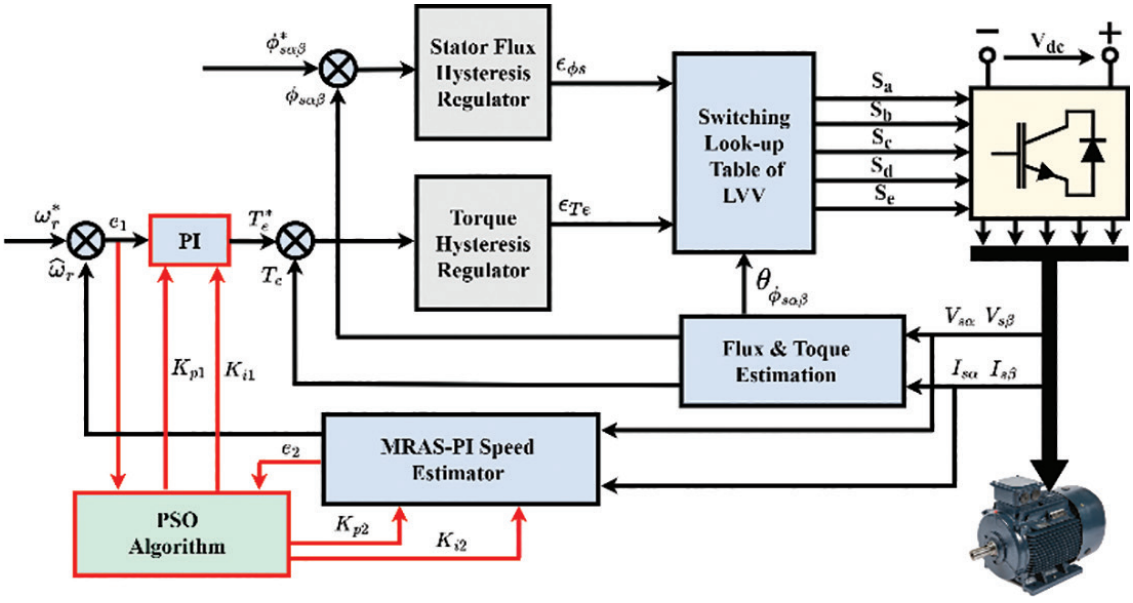

Fig. 8. Block diagram of the proposed speed sensorless control (DTC-MRAS-PSO/PI) of five-phase induction motor. DTC, direct torque control; MRAS, model reference adaptive system; PI, proportional-integral; PSO, particle swarm optimisation.

PI controller parameters in the adaptation mechanism of the MRAS estimator. In addition, a further investigation will be carried out in the speed regulator loop, based on optimising the gains of the classical PI controller using the PSO algorithm to obtain a fast response of speed and electromagnetic torque and compensating for the sensorless DTC of the five-phase induction motor (DTC-MRAS-PSO\PI), as shown in Figure 8. In this paper, an integral of the time-weighted absolute error (ITAE) has been chosen as an objective function to evaluate the performance of classical PI controllers. There are a large number of published investigations proving the effectiveness of the error function (ITAE) in optimisation algorithms (Idir et al., 2022). Eq. (15) defines the value of the ITAE as:

$$J\left(K_p, K_i\right) = \int_0^{t_{sim}} t\left|e(t)\right| dt \tag{15}$$

The steps for execution of the PSO algorithm to optimise the classical PI controller parameters are as follows.

Algorithm: PSO Algorithm to optimise the classical PI controller
Begin
Step 1. Initialise the PSO parameters.
Step 2. Generate the parameters of the FOPI controller randomly.
Step 3. Execute DTC control of the five-phase induction motor.
Step 4. Evaluate and calculate the value of the fitness function (ITAE).
Step 5. Execute the selection, crossover and mutation steps.
Step 6. Generate the optimum values of Kp1, Ki1, Kp2 and Ki2.
Step 7. Repeat Step 3 until the maximum number of iterations has been reached.
Step 8. Print the optimum solutions of Kp1, Ki1, Kp2 and Ki2.
End

4. Intelligent Fractional Order Controller-Based MRAS Speed Estimator

4.1. Fractional order systems

FC is a field of mathematics that generalises the operations of derivation and integration to non-integer orders. Where n is irrational, fractional or complex, n-fold integrals are more easily solved with FC. The generalised fundamental operator is used for differentiation and integration and is written as follows:

$$aD_t^{\alpha} = \begin{cases} \dfrac{d^{\alpha}}{dt^{\alpha}}, & R(\alpha) > 0 \\ 1, & R(\alpha) = 0 \\ \int_a^t (d\tau)^{-\alpha}, & R(\alpha) < 0 \end{cases} \tag{16}$$

where a is integration lower limit, t is integration upper limit and α is fractional differentiation or integration order.

Generally, fractional differentiation is considered for $\alpha \in R$, but it can also be extended to complex numbers. There are several definitions of fractional differentiation, one of the most common being the Riemann–Liouville differential defined as follows:

$$aD_t^{-\alpha} f(t) = \frac{1}{\Gamma(\alpha)} \int_a^t (t-\tau)^{\alpha-1} f(\tau) d\tau \tag{17}$$

where $0 < \alpha < 1$ and a is the first-time instance.

It is essential to find integer-order approximations for fractional-order transfer functions. In other words, when running simulations or implementing correctors, the fractional order transfer functions must be replaced by integer order transfer functions that exhibit similar behaviour but are much easier to manipulate. Note that the approximations available in the 's' frequency domain are called analogue approximations.

In this paper, the Oustaloup approximation method was chosen to approximate the fractional-order integrator and differentiator (Oustaloup et al., 2000). The purpose of this method is to achieve an accurate approximation of a fractional operator as:

$$G(s) = S^{\alpha}, \ (\alpha \in R) \tag{18}$$

The standard Oustaloup filter takes the following form:

$$G(s) = K \prod_{k=1}^{N} \frac{s + \omega_k'}{s + \omega_k} \tag{19}$$

where the zeros, poles and gain can be obtained from:

$$\omega_k = \omega_b.\omega_u^{(2k-1+\gamma)/N}, \omega_k^{'} = \omega_b.\omega_u^{(2k-1-\gamma)/N}, K = \omega_h^{\gamma} \tag{20}$$

For $k = 1,2,...,N$ with, $\omega_u = \sqrt{\omega_h/\omega_b}$. Where ω_b, ω_h are the lower and upper bounds in the frequency desired interval and γ, N are the order of derivative and filter, respectively.

4.2. Proposed DTC-MRAS-PSO\FOPI scheme

Most investigations on the MRAS estimator have focused only on using the classical PI controller in the adaptation mechanism due to their simple basic design, which only requires adjustment of the two parameters Kp and Ki of the corrector transfer function, as shown in Eq. (21). In this paper, the FOPI controller can be more of benefit for the dynamic response of sensorless DTC for the five-phase induction motor (DTC-MRAS-PSO\FOPI). The FOPI controller is an extension of the classical PI controller, offering an additional degree of liberty λ, where λ can be any positive real integer (Eq. 22).

$$G_{PI}(s) = K_p + K_i s^{-1} \tag{21}$$

$$G_{FOPI}(s) = K_p + K_i s^{-\lambda} \tag{22}$$

Since each FOPI controller has three parameters, there are a total of six parameters to be optimised with the PSO algorithm. The PSO algorithm searches the set of controller parameters in a six-dimensional space. Each particle contains six elements that assign real values. Eq. (23) shows the order of a particle as:

$$P_i = \left[K_{p1}, K_{i1}, \lambda_1, K_{p2}, K_{i2}, \lambda_2\right] \tag{23}$$

where K_{p1}, K_{p1} and λ_1 are the first FOPI controller parameters of the speed control loop. K_{p2}, K_{i2} and λ_2 are the second FOPI controller parameters of the adaptation mechanism.

Figure 9 shows the optimisation diagram by the PSO algorithm in sensorless DTC based on the FOPI regulator for the five-phase induction motor.

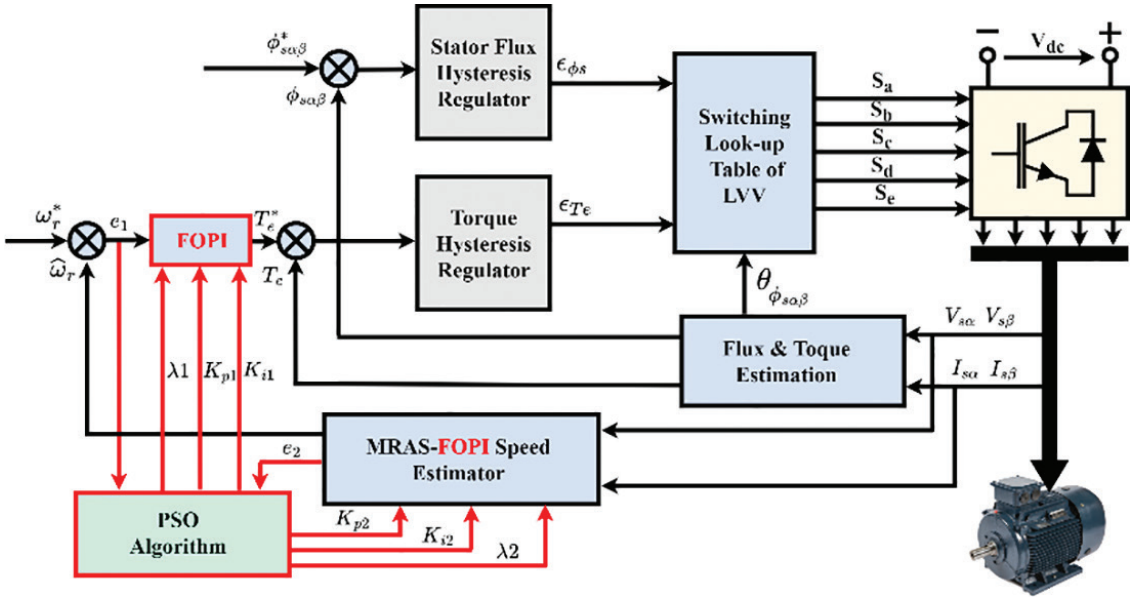

Fig. 9. Block diagram of speed sensorless control (DTC-MRAS-PSO/FOPI) of five-phase induction motor. DTC, direct torque control; FOPI, fractional-order proportional-integral; MRAS, model reference adaptive system; PSO, particle swarm optimisation.

The steps for execution of the PSO algorithm to optimise the FOPI controller parameters are as follows.

Algorithm: PSO Algorithm to optimise the FOPI controller
Begin
Step 1. Initialise the PSO parameters.
Step 2. Generate the parameters of the FOPI controller randomly.
Step 3. Execute DTC control of the five-phase induction motor.
Step 4. Evaluate and calculate the value of the fitness function (ITAE).
Step 5. Execute the selection, crossover and mutation steps.
Step 6. Generate the optimum values of Kp1, Ki1, λ1, Kp2, Ki2 and λ2.
Step 7. Repeat Step 3 until the maximum number of iterations has been reached.
Step 8. Print the optimum solutions of Kp1, Ki1, λ1, Kp2, Ki2 and λ2.
End

5. Simulation Results

To validate and evaluate the performance of the sensorless DTC structure based on MRAS speed estimation techniques (conventional DTC-MRAS-PI, proposed DTC-MRAS-PSO/PI and proposed DTC-MRAS-PSO/FOPI) applied to a five-phase induction machine, simulations have been carried out. The nominal values and parameters of the five-phase induction machine can be found in Table 2. The reference torque is given by the speed loop. Table 3 gives the parameters of the classical PI regulator (PI-1 and PI-2) and the fractional-order PI regulator (FOPI-1 and FOPI-2) for the different techniques studied in this paper. Table 4 shows the parameters of the PSO algorithm. Note that the optimisation process converges after several hours of simulation to obtain optimal values for the controller parameters (PSO/PI-1, PSO/PI-2, PSO/FOPI-1 and PSO/FOPI-2).

The PSO/FOPI-1 controller used in the speed regulator loop is given as:

$$G_{PSO/FOPI-1}(s) = 2.351 + 5.802\mathrm{s}^{-0.784} \tag{24}$$

Designation	Notations	Rating values	Unity
Stator resistance	Rs	10	[Ω]
Rotor resistance	Rr	6.3	[Ω]
Stator inductance	Ls	0.4642	[H]
Rotor inductance	Lr	0.4612	[H]
Moment of inertia	J	0.4212	[kg/m²]
Friction coefficient	F	0.0001	/
Number of poles	P	2	/

Table 2. Five-phase induction motor parameters.

Technique studied	Controller type	Kp1	Ki1	λ1	Kp2	Ki2	λ2
DTC-MRAS-PI	PI controller	1.5	10	1	50	50000	1
DTC-MRAS-PSO/PI	PSO with PI controller	1.9121	7.7547	1	42.2352	97235	1
DTC-MRAS-PSO/FOPI	PSO with FOPI controller	2.351	5.802	0.784	22.164	57012.179	0.813

DTC, direct torque control; FOPI, fractional-order proportional-integral; MRAS, model reference adaptive system; PI, proportional-integral; PSO, particle swarm optimisation.

Table 3. Gain parameters of the controller for different techniques.

Consequently, the transfer function of PSO/FOPI-1 using the Oustaloup approach with $\omega_b = 0.001$ rad/s, $\omega_h = 1000$ rad/s and N = 5 is given as follows:

$$G_{PSO/FOPI-1}(s) = \frac{2.377s^5 + 233.8s^4 + 2110s^3 + 3226s^2 + 534.9s + 5.812}{s^5 + 90.76s^4 + 488.9s^3 + 165.5s^2 + 3.521s + 0.004446} \quad (25)$$

The PSO/FOPI-2 controller used in the adaptation mechanism is given as follows:

$$G_{PSO/FOPI-2}(s) = 22.164 + 57012.179s^{-0.813} \quad (26)$$

Consequently, the transfer function of PSO/FOPI-2 using the Oustaloup approach with $\omega_b = 0.001$ rad/s, $\omega_h = 1000$ rad/s and N = 5 is given as follows:

$$G_{PSO/FOPI-2}(s) = \frac{229.6s^5 + 173000s^4 + 8378000s^3 + 25730000s^2 + 4971000s + 57010}{s^5 + 87.2s^4 + 451.3s^3 + 146.8s^2 + 3s + 0.003639} \quad (27)$$

Figures 10–20 show the simulation results obtained by speed sensorless DTC based on the different techniques of MRAS observer (DTC-MRAS-PI, DTC-MRAS-PSO/PI and DTC-MRAS-PSO/FOPI) for the five-phase induction machine. These simulations are carried out in a variable reference speed range (which contains the reverse of the speed direction) with a fixed load torque.

It can be seen that the variation of the rotor speed reference is divided into four main segments: from 0 s to 0.5 s is the first segment (transient state), the second segment is defined as 0.5 s to 1.5 s (steady state), from 1.5 s to 2.5 s is the third segment (transient state) and the remainder is the fourth segment (steady state). The first and second

Parameter	Value
Population size	30
Maximum cycle number	70
Lower bound for [kp1–2; ki1–2; 1–2]	[0.001;0.001;0.001]
Upper bound for [kp1–2, ki1–2, 1–2]	[50;500;2]

FOPI, fractional-order proportional-integral; PI, proportional-integral; PSO, particle swarm optimisation.

Table 4. PSO of (PI and FOPI) parameters for solving optimisation problems.

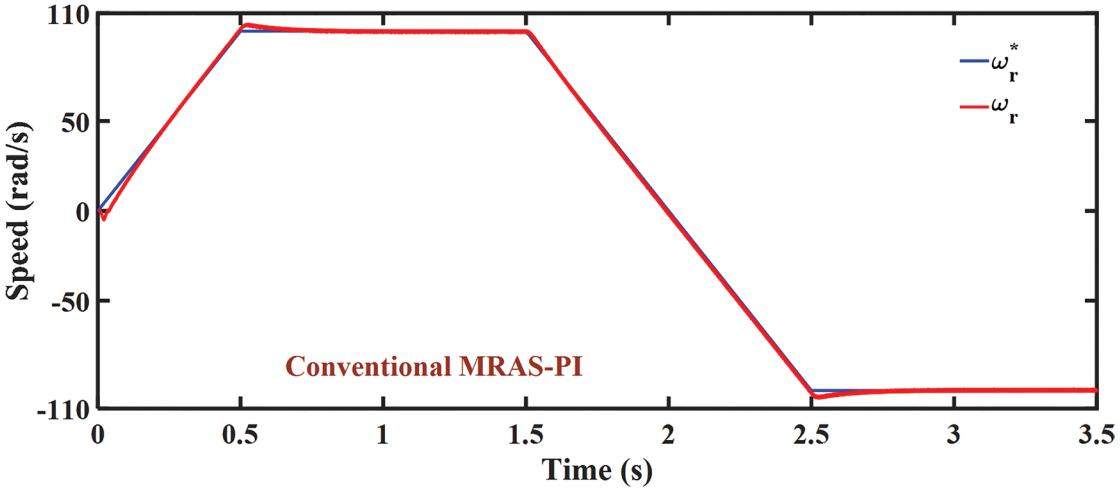

Fig. 10. Rotor speed (reference speed in blue, Estimated speed in red) of conventional DTC-MRAS-PI. DTC, direct torque control; MRAS, model reference adaptive system; PI, proportional-integral.

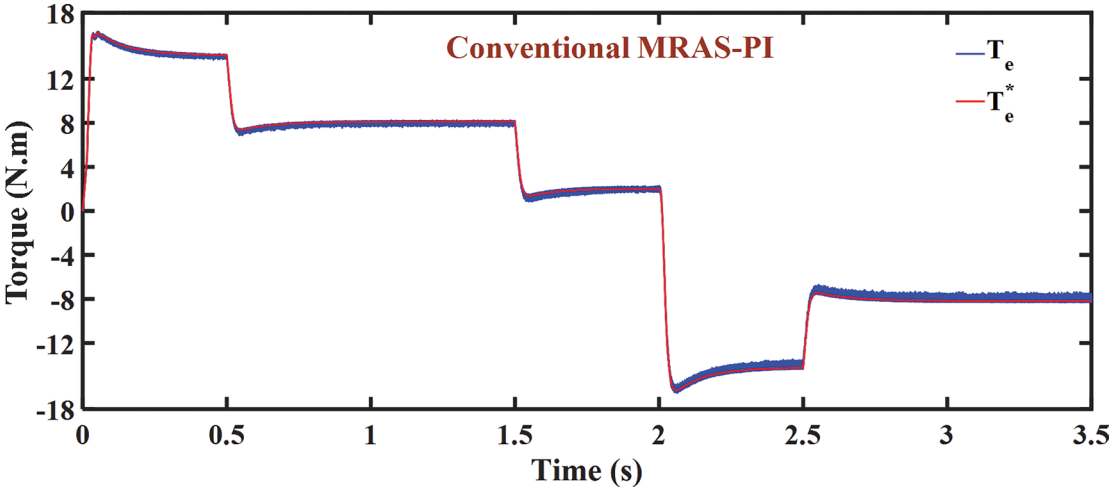

Fig. 11. Electromagnetic torque (reference torque in red, Estimated torque in blue) of conventional DTC-MRAS-PI. DTC, direct torque control; MRAS, model reference adaptive system; PI, proportional-integral.

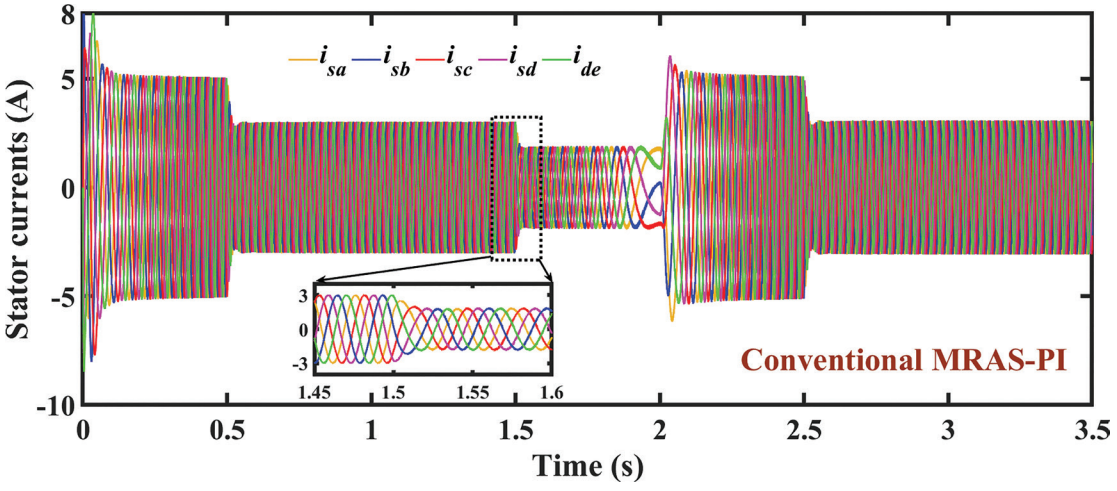

Fig. 12. Stator current of conventional DTC-MRAS-PI. DTC, direct torque control; MRAS, model reference adaptive system; PI, proportional-integral.

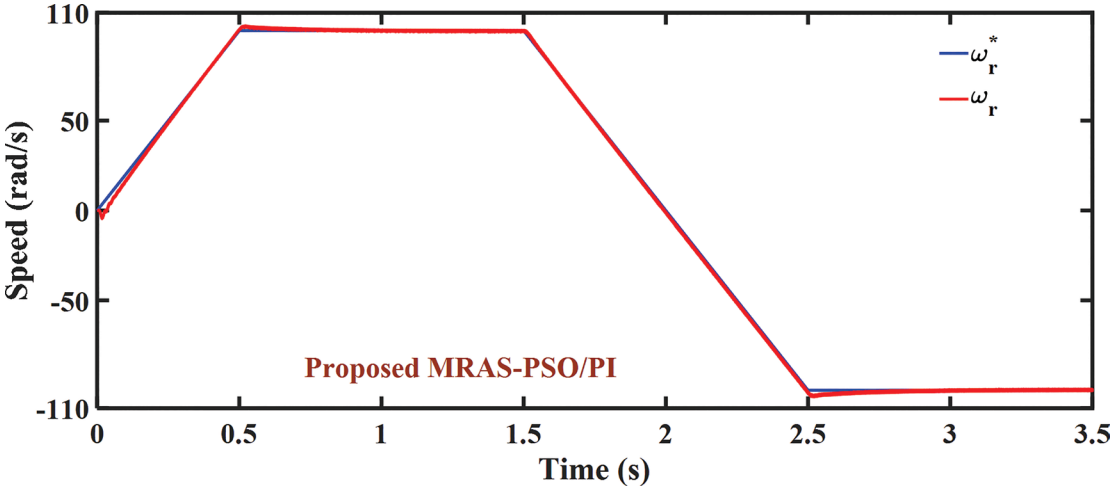

Fig. 13. Rotor speed (reference speed in blue, estimated speed in red) of proposed DTC-MRAS-PSO/PI. DTC, direct torque control; MRAS, model reference adaptive system; PI, proportional-integral; PSO, particle swarm optimisation.

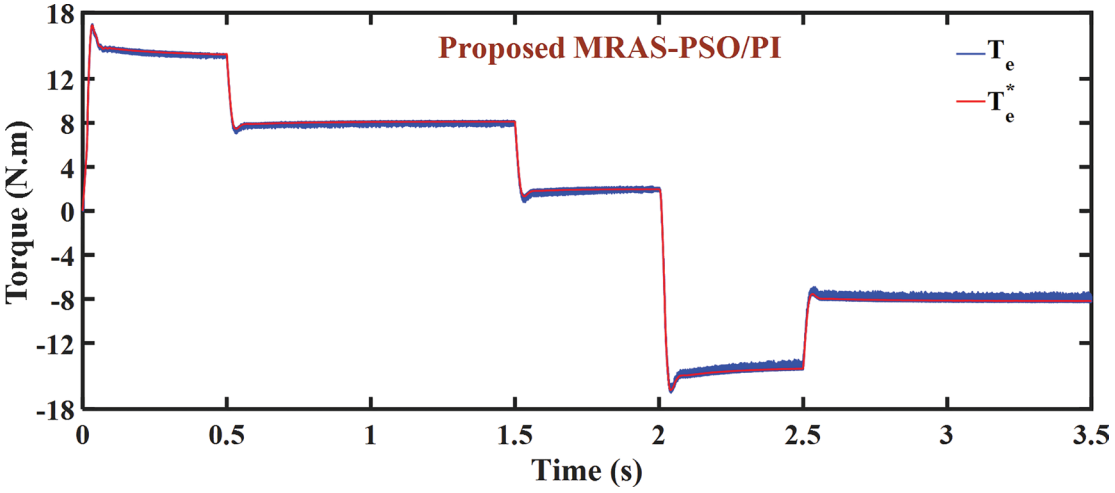

Fig. 14. Electromagnetic torque (reference torque in red, Estimated torque in blue) of proposed DTC-MRAS-PSO/PI. DTC, direct torque control; MRAS, model reference adaptive system; PI, proportional-integral; PSO, particle swarm optimisation.

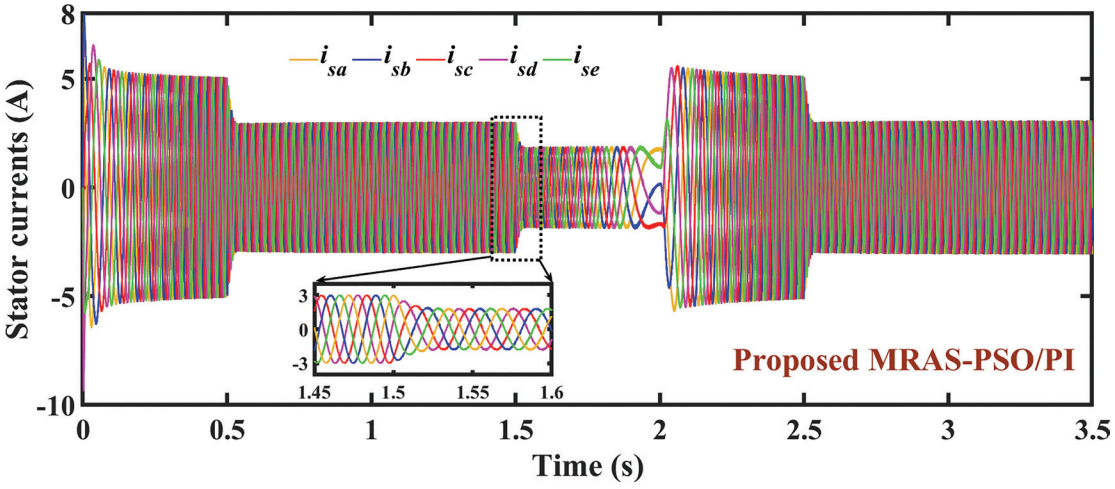

Fig. 15. Stator current of proposed DTC-MRAS-PSO/PI. DTC, direct torque control; MRAS, model reference adaptive system; PI, proportional-integral; PSO, particle swarm optimisation.

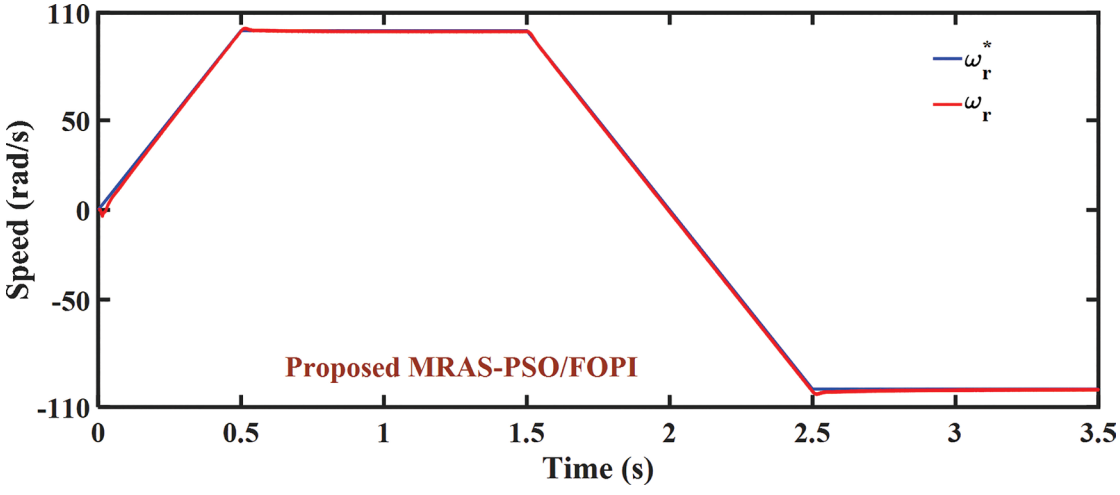

Fig. 16. Rotor speed (reference speed in blue, estimated speed in red) of proposed DTC-MRAS-PSO/FOPI. DTC, direct torque control; FOPI, fractional-order proportional-integral; MRAS, model reference adaptive system; PSO, particle swarm optimisation.

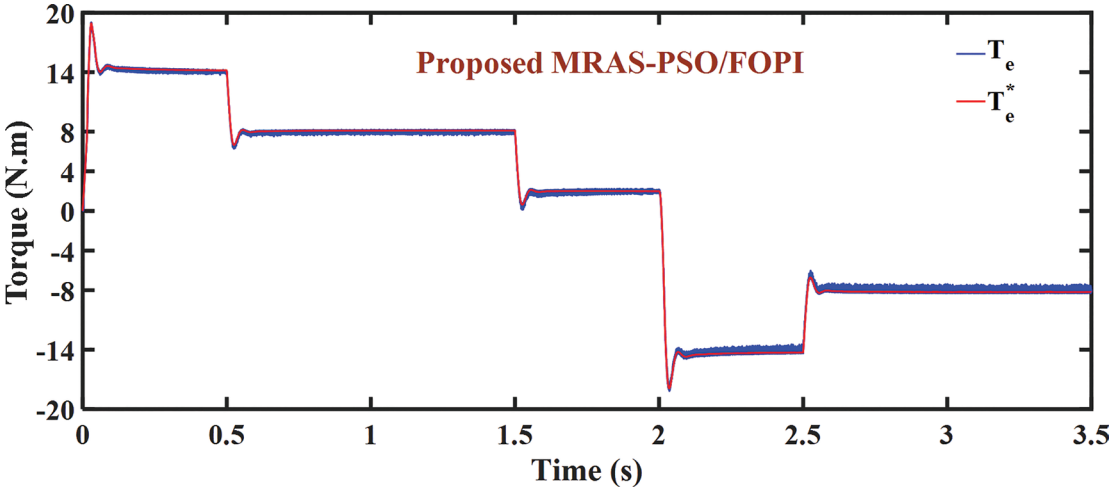

Fig. 17. Electromagnetic torque (reference torque in red, estimated torque in blue) of proposed DTC-MRAS-PSO/FOPI. DTC, direct torque control; FOPI, fractional-order proportional-integral; MRAS, model reference adaptive system; PSO, particle swarm optimisation.

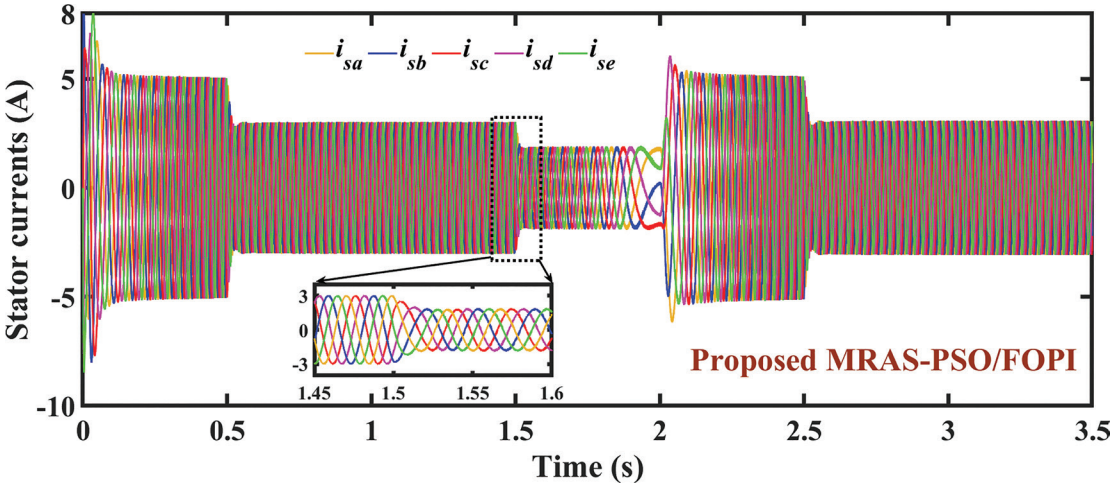

Fig. 18. Stator current of proposed DTC-MRAS-PSO/FOPI. DTC, direct torque control; FOPI, fractional-order proportional-integral; MRAS, model reference adaptive system; PSO, particle swarm optimisation.

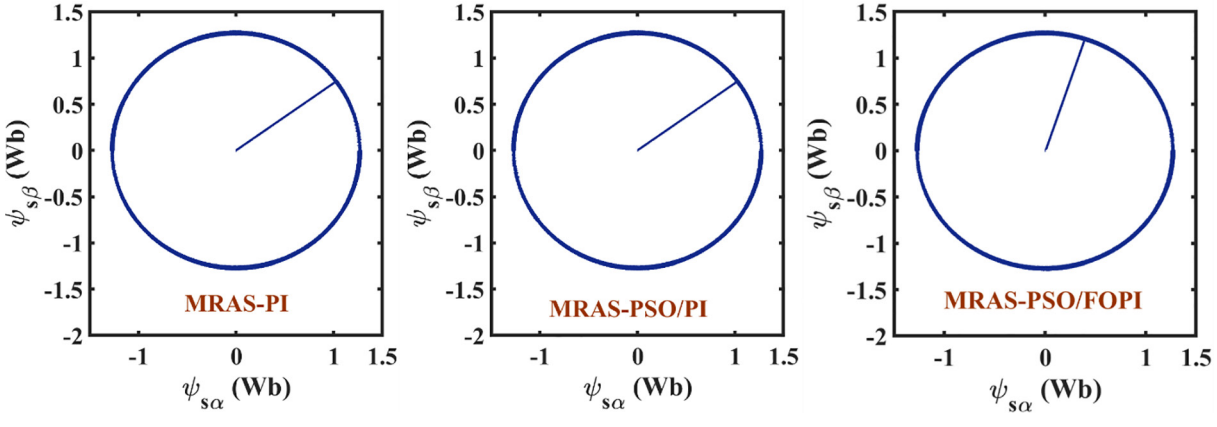

Fig. 19. Stator flux in α-β subspace: left side-(conventional DTC-MRAS-PI), center side-(proposed DTC-MRAS-PSO/PI) and right side-(proposed DTC-MRAS-PSO/FOPI). DTC, direct torque control; FOPI, fractional-order proportional-integral; MRAS, model reference adaptive system; PI, proportional-integral; PSO, particle swarm optimisation.

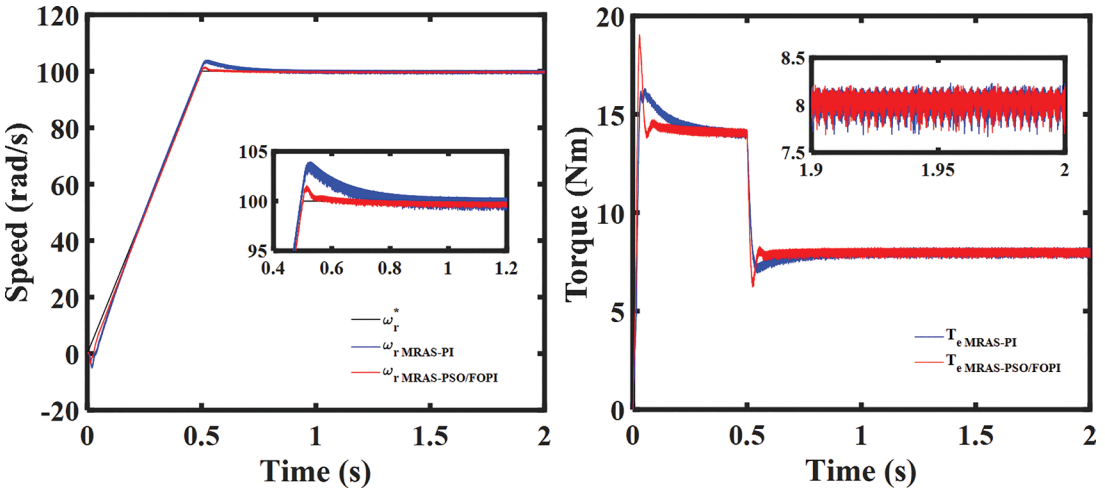

Fig. 20. Comparative study between proposed DTC-MRAS-PSO/FOPI and conventional DTC-MRAS-PI) for a 25% nominal stator resistance value (left side – speed and right side – torque). DTC, direct torque control; FOPI, fractional-order proportional-integral; MRAS, model reference adaptive system; PI, proportional-integral; PSO, particle swarm optimisation.

segments are in the forward direction phase, while the third and fourth segments define the reverse direction of rotor rotation.

Figure 10 shows the estimated speed response of the conventional DTC-MRAS-PI, which converges towards the reference speed with a reasonably significant overshoot. The rotational speed of the rotor of the five-phase induction motor precisely follows the speed variation with an error that may be negligible in a steady state. In contrast, an error is observable in transient regimes. From the results obtained in Figure 13, it can be seen that the speed estimator proposed using the PSO algorithm in DTC-MRAS-PSO/PI offers a better-estimated speed response compared with the DTC-MRAS-PI estimator, particularly in terms of reduced error and overshoot compared with conventional DTC-MRAS-PI. As shown in Figure 16, the best sensorless control for speed estimation is obtained using the proposed FOPI controller with the Oustaloup approximation, as it has a more stable structure. Thus, the proposed DTC-MRAS-PSO/FOPI offers accurate speed following the stable segment with near-zero error and low overshoot in the transient regime.

Figures 11, 14 and 17 show the electromagnetic torque developed DTC techniques based on MRAS speed estimator. It is evident that the torque developed follows its reference value. Furthermore, it is clear that all techniques present torque ripples due to the presence of the hysteresis regulator. Consequently, the DTC-MRAS-PSO/FOPI has reduced ripples than the conventional DTC-MRAS-PI and the proposed DTC-MRAS-PSO/PI, leading to more stable operation.

The stator currents of the five-phase induction machine for different approaches (DTC-MRAS-PI, DTC-MRAS-PSO/PI and DTC-MRAS-PSO/FOPI) are shown in Figures 12, 15 and 18. It is clear that stator currents perform according to the dynamics of speed variation and applied load torque. Moreover, significantly high stator currents are observed during the start-up phase and in the rotor reversal segment due to the electromagnetic torque developed by the five-phase induction motor. As the zoomed-in area in Figures 12, 15 and 18 shows, motor phase currents are balanced for all three techniques examined.

Figure 19 illustrates the circular trajectory of the stator flux vector amplitude in the (α–β) subspace for the different approaches. It can be observed that the stator flux does not exceed the limits of its band. Moreover, variations in rotor speed do not affect the stator flux, especially during transient phases, which confirm the dynamics of the studied methods (conventional DTC-MRAS-PI, proposed DTC-MRAS-PSO/PI and proposed DTC-MRAS-PSO/FOPI).

Figures 20–27 show the motor responses in the event of stator resistance variations. As can be seen, the proposed DTC-MRAS-PSO/FOPI technique shows the best response when the stator resistance increases from 25% to 150%. The various simulation results confirm that using the FOPI controller as an adaptation mechanism for the MRAS estimator provides good behaviour of the five-phase motor drive. Indeed, the estimated speed and torque show fewer ripples, but they ensuring good tracking during stator resistance variations.

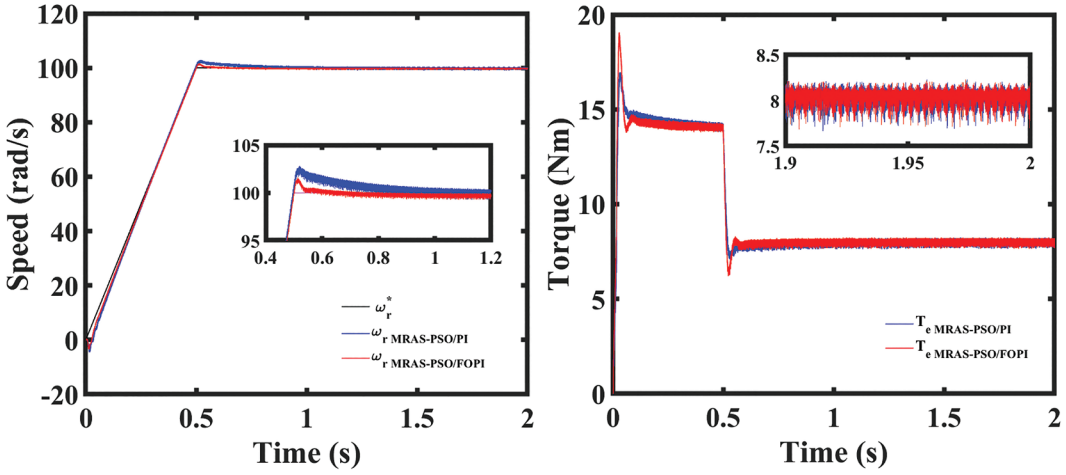

Fig. 21. Comparative study between proposed DTC-MRAS-PSO/FOPI and Proposed DTC-MRAS-PSO/PI) for a 25% nominal stator resistance value (left side – speed and right side – torque). DTC, direct torque control; FOPI, fractional-order proportional-integral; MRAS, model reference adaptive system; PI, proportional-integral; PSO, particle swarm optimisation.

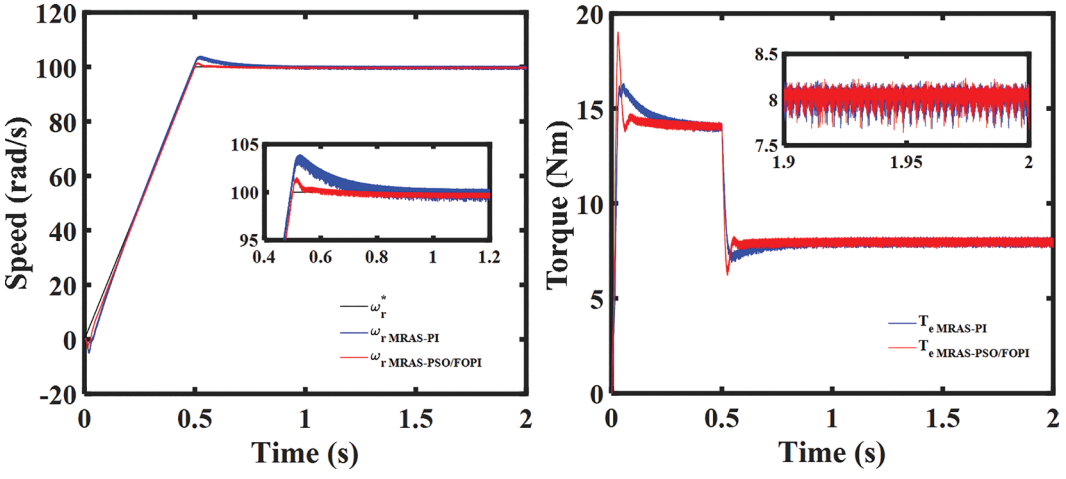

Fig. 22. Comparative study between proposed DTC-MRAS-PSO/FOPI and conventional DTC-MRAS-PI) for a 50% nominal stator resistance value (left side – speed and right side – torque). DTC, direct torque control; FOPI, fractional-order proportional-integral; MRAS, model reference adaptive system; PI, proportional-integral; PSO, particle swarm optimisation.

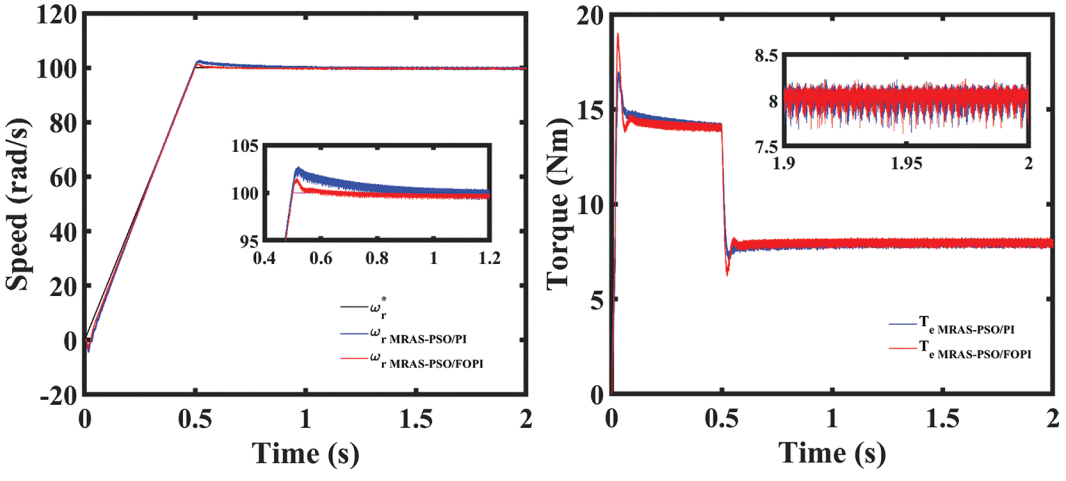

Fig. 23. Comparative study between proposed DTC-MRAS-PSO/FOPI and Proposed DTC-MRAS-PSO/PI) for a 50% nominal stator resistance value (left side – speed and right side – torque). DTC, direct torque control; FOPI, fractional-order proportional-integral; MRAS, model reference adaptive system; PI, proportional-integral; PSO, particle swarm optimisation.

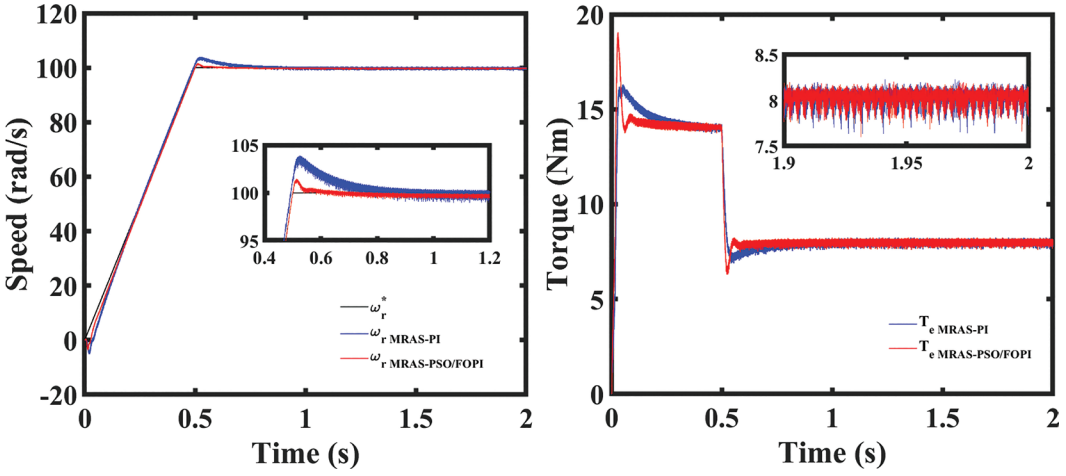

Fig. 24. Comparative study between proposed DTC-MRAS-PSO/FOPI and conventional DTC-MRAS-PI) for a 100% nominal stator resistance value (left side – speed and right side – torque). DTC, direct torque control; FOPI, fractional-order proportional-integral; MRAS, model reference adaptive system; PI, proportional-integral; PSO, particle swarm optimisation.

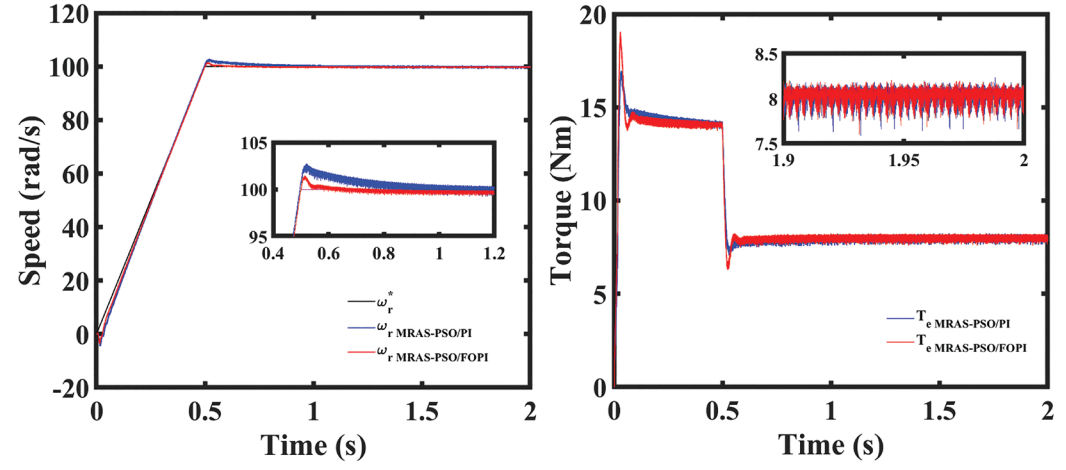

Fig. 25. Comparative study between proposed DTC-MRAS-PSO/FOPI and Proposed DTC-MRAS-PSO/PI) for a 100% nominal stator resistance value (left side – speed and right side – torque). DTC, direct torque control; FOPI, fractional-order proportional-integral; MRAS, model reference adaptive system; PI, proportional-integral; PSO, particle swarm optimisation.

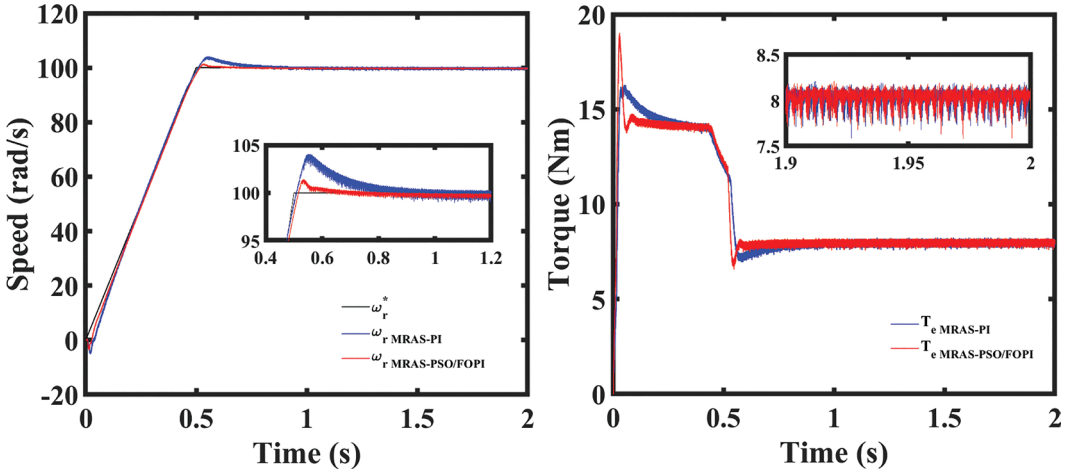

Fig. 26. Comparative study between proposed DTC-MRAS-PSO/FOPI and conventional DTC-MRAS-PI) for a 150% nominal stator resistance value (left side – speed and right side – torque). DTC, direct torque control; FOPI, fractional-order proportional-integral; MRAS, model reference adaptive system; PI, proportional-integral; PSO, particle swarm optimisation.

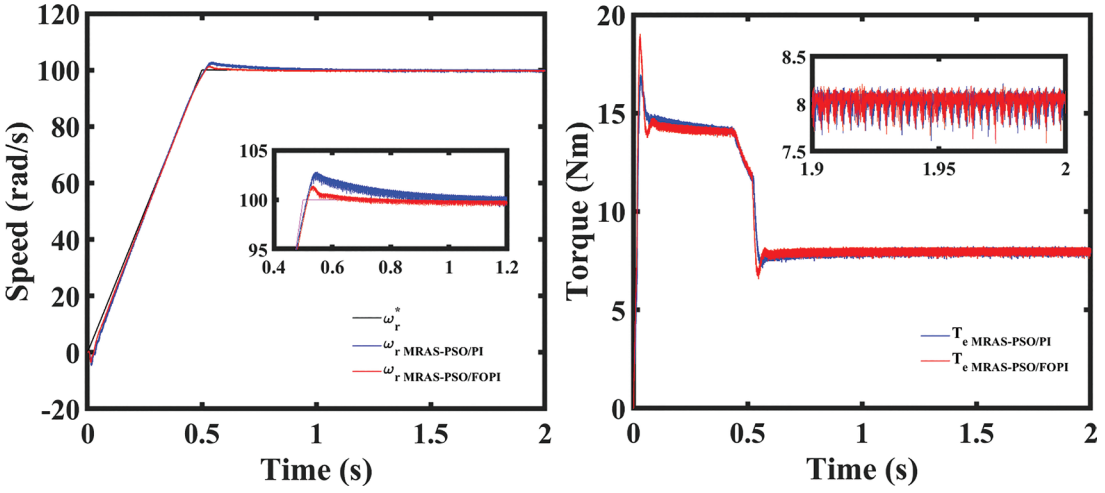

Fig. 27. Comparative study between proposed DTC-MRAS-PSO/FOPI and Proposed DTC-MRAS-PSO/PI) for a 150% nominal stator resistance value (left side – speed and right side – torque). DTC, direct torque control; FOPI, fractional-order proportional-integral; MRAS, model reference adaptive system; PI, proportional-integral; PSO, particle swarm optimisation.

Based on these comparisons, it is reasonable to conclude that the MRAS estimator is adapted to DTC for the five-phase induction machine. Combining the PSO algorithm with the classical PI controller improves robustness compared with the conventional MRAS. Then, the FOPI controller with the PSO algorithm proves to be one of the most robust and appropriate controls for better performance.

6. Conclusion

This paper proposes an adaptive mechanism of the MRAS observer based on fractional order controller and PSO algorithm applied to speed sensorless DTC for the five-phase induction motor. Moreover, the developed control used the PSO algorithm to optimise the gains of the fractional order controller used in the speed regulator loop to improve the dynamic performance of system. In addition, a comparative investigation has been carried out of the different techniques studied in this paper, under different operating conditions, of which the proposed fractional design presents a promising solution in the sensorless control of the five-phase induction motor. Regarding the obtained results, it can be concluded that the MRAS estimator is adapted to the DTC for the five-phase induction machine. To enhance the senseless DTC, a combination of the PSO algorithm with the fractional order controller can widely provide good adynamic stability, eliminating rotor speed overshoot, improving response time and minimising torque ripple.

In future work, the proposed methods can be implemented in an experimental test bench and compared with the results of the present paper. Other fractional order systems and artificial neural networks can be also used to improve speed sensorless DTC for multiphase motors.

References

Abd Samat, A. A., Ishak, D., Omar, A. M., Iqbal, S. and Razak, M. A. (2016). A New Speed Sensorless Field-Oriented Controller for PMSM Based on MRAS and PSO. *Journal of Electrical Systems*, 12(3), pp. 566–573.

Agarwal, J., Parmar, G., Gupta, R. and Sikander, A. (2018). Analysis of Grey Wolf Optimizer Based Fractional Order PID Controller in Speed Control of DC Motor. *Microsystem Technologies*, 24, pp. 4997–5006. doi: 10.1007/s00542-018-3920-4.

Astrom, K. J. (1996). Adaptive Control Around 1960. *IEEE Control Systems Magazine*, 16(3), pp. 44–49. doi: 10.1109/37.506397.

Bahloul, M., Vargas, A. N., Chrifi-Alaoui, L., Drid, S. and Chaabane M. (2019). Modified Robust Model Reference Adaptive System Scheme for a Speed

Sensorless Vector Control of Induction Motor. In: *Proceedings of the 19th International Conference on Sciences and Techniques of Automatic Control and Computer Engineering STA*. Sousse, Tunisia, 24-26March2019.doi:10.1109/STA.2019.8717213.

Bermudez, M., Gonzalez-Prieto, I., Barrero, F., Guzman, H., Kestelyn, X. and Duran, M. J. (2018). An Experimental Assessment of Open-Phase Fault-Tolerant Virtual-Vector-Based Direct Torque Control in Five-Phase Induction Motor Drives. *IEEE Transactions on Power Electronics*, 33(3), pp. 2774–2784. doi: 10.1109/TPEL.2017.2711531.

Boztas, G. and Aydogmus, O. (2022). Implementation of Sensorless Speed Control of Synchronous Reluctance Motor using Extended Kalman Filter. *Engineering Science and Technology, an International Journal*, 31, p. 101066. doi: 10.1016/j.jestch.2021.09.012.

Das, S., Pan, I. and Das, S. (2013). Performance Comparison of Optimal Fractional Order Hybrid Fuzzy PID Controllers for Handling Oscillatory Fractional Order Processes with Dead Time. *ISA Transactions*, 52(4), pp. 550–566. doi: 10.1016/j.isatra.2013.03.004.

Duran, M. J., Gonzalez-Prieto, I., Rios-Garcia, N. and Barrero, F. (2017). A Simple, Fast, and Robust Open-Phase Fault Detection Technique for Six-Phase Induction Motor Drives. *IEEE Transactions on Power Electronics*, 33(1), pp. 547–557. doi: 10.1109/TPEL.2017.2670924.

Ekinci, S., Hekimoğlu, B. and Izci, D. (2021). Opposition Based Henry Gas Solubility Optimization as a Novel Algorithm for PID Control of DC Motor. *Engineering Science and Technology, an International Journal*, 24(2), pp. 331–342. doi: 10.1016/j.jestch.2020.08.011.

El Ouanjli, N., Mahfoud, S., Bhaskar, M. S., El Daoudi, S., Derouich, A. and El Mahfoud, M. (2022). A New Intelligent Adaptation Mechanism of MRAS Based on a Genetic Algorithm Applied to Speed Sensorless Direct Torque Control for Induction Motor. *International Journal of Dynamics and Control*, 10(6), pp. 2095–2110. doi: 10.1007/s40435-022-00947-z.

Gharehchopogh, F. S. and Gholizadeh, H. (2019). A Comprehensive Survey: Whale Optimization Algorithm and its Applications. *Swarm and Evolutionary Computation*, 48, pp. 1–24. doi: 10.1016/j.swevo.2019.03.004.

González-Prieto, I., Durán, M. J., Bermúdez, M., Barrero, F. and Martín, C. (2019a). Assessment of Virtual-Voltage-based Model Predictive Controllers in Six-Phase Drives Under Open-Phase Faults. *IEEE Journal of Emerging and Selected Topics in Power Electronics*, 8(3), pp. 2634–2644. doi: 10.1109/JESTPE.2019.2915666.

González-Prieto, I., Zoric, I., Duran, M. J. and Levi, E. (2019b). Constrained Model Predictive Control in Nine-Phase Induction Motor Drives. *IEEE Transactions on Energy Conversion*, 34(4), pp. 1881–1889. doi: 10.1109/TEC.2019.2929622.

Guedida, S., Tabbache, B., Nounou, K. and Benbouzid, M. (2023). Direct Torque Control Scheme for Less Harmonic Currents And Torque Ripples For Dual Star Induction Motor. *Revue Roumaine des Sciences Techniques—Série Électrotechnique Et Énergétique*, 68(4), pp. 331–338. doi: 10.59277/RRST-EE.2023.4.2.

Han, D. and Zhang, Y. (2019). The Speed estimation based on MRAS Induction motor. In: *Proceedings of the IEEE 3rd Advanced Information Management, Communicates, Electronic and Automation Control Conference IMCEC*. Chongqing, China, 11-13 October 2019. doi: 10.1109/IMCEC46724.2019.8984140.

He, C. Xiong, H. and Shen, Z. (2021). Current Loop Control Strategy of PMSM Based on Fractional Order PID Control Technology. In: *Proceedings of the 6th Asia Conference on Power and Electrical Engineering*. Chongqing, China, 08-11 April 2021. doi: 10.1109/ACPEE51499.2021.9436899.

Holakooie, M. H., Ojaghi, M. and Taheri, A. (2018). Modified DTC of a Six-Phase Induction Motor with a Second-Order Sliding-Mode MRAS-Based Speed Estimator. *IEEE Transactions on Power Electronics*, 34(1), pp. 600–611. doi: 10.1109/TPEL.2018.2825227.

Idir, A., Canale, L., Bensafia, Y. and Khettab, K. (2022). Design and Robust Performance Analysis of Low-Order Approximation of Fractional PID Controller Based on an IABC Algorithm for an Automatic Voltage Regulator System. *Energies*, 15(23), p. 8973. doi: 10.3390/en15238973.

Kennedy, J. and Eberhart, R. C. (1997). A discrete binary version of the particle swarm algorithm. In: *Proceedings of the IEEE International Conference on Systems, Man, and Cybernetics. Computational Cybernetics and Simulation*. Orlando, FL, USA, 12-15 October 1997. doi: 10.1109/ICSMC.1997.637339.

Khalilpour, M., Razmjooy, N., Hosseini, H. and Moallem, P. (2011). Optimal control of DC motor using invasive weed optimization (IWO) algorithm. In: *Majlesi Conference on Electrical Engineering*, Majlesi New Town, Isfahan, Iran.

Kim, N. H. and Kim, M. H. (2009). Modified Direct Torque Control System of Five Phase Induction Motor. *Journal of Electrical Engineering and Technology*, 4(2), pp. 266–271. doi: 10.5370/JEET.2009.4.2.266.

Krim, S. and Mimouni, M. F. (2023). Design and Xilinx Virtex-Field-Programmable Gate Array for Hardware in the Loop of Sensorless Second-Order Sliding Mode Control and Model Reference Adaptive System–Sliding Mode Observer for Direct Torque Control Of Induction Motor Drive. *Proceedings of the Institution of Mechanical Engineers. Part I: Journal of Systems and Control Engineering*, 237(5), pp. 839–869.

Levi, E. (2008). Multiphase Electric Machines for Variable-Speed Applications. *IEEE Transactions on Industrial Electronics*, 55(5), pp. 1893–1909. doi: 10.1109/TIE.2008.918488.

Liu, Z., Li, Y. and Zheng, Z. (2018). A Review of Drive Techniques for Multiphase Machines. *CES Transactions on Electrical Machines and Systems*, 2(2), pp. 243–251. doi: 10.30941/CESTEMS.2018.00030.

Martin, C., Bermúdez, M., Barrero, F., Arahal, M. R., Kestelyn, X. and Durán, M. J. (2017). Sensitivity of Predictive Controllers to Parameter Variation in Five-Phase Induction Motor Drives. *Control Engineering Practice*, 68, pp. 23–31. doi: 10.1016/j.conengprac.2017.08.001.

Oustaloup, A., Levron, F., Mathieu, B. and Nanot, F. M. (2000). Frequency-Band Complex Noninteger Differentiator: Characterization and Synthesis. *IEEE Transactions on Circuits and Systems I: Fundamental Theory and Applications*, 47(1), pp. 25–39. doi: 10.1109/81.817385.

Pavithran, K. N., Parimelalagan, R. and Krishnamurthy, M. R. (1988). Studies on Inverter-Fed Five-Phase Induction Motor Drive. *IEEE Transactions on Power Electronics*, 3(2), pp. 224–235. doi: 10.1109/63.4353.

Razzaghian, A., Kardehi Moghaddam, R. and Pariz, N. (2022). Adaptive Neural Network Conformable Fractional-Order Nonsingular Terminal Sliding Mode Control for a Class of Second-Order Nonlinear Systems. *IETE Journal of Research*, 68(6), pp. 4290–4299. doi: 10.1080/03772063.2020.1791743.

Reddy, V. S. and Devabhaktuni, S. (2022). Enhanced Low-Speed Characteristics with Constant Switching Torque Controller-Based DTC Technique of Five-Phase Induction Motor Drive with FOPI Control. *IEEE Transactions on Industrial Electronics*, 70(11), pp. 10789–10799. doi: 10.1109/TIE.2022.3227275.

Rigatos, G., Abbaszadeh, M., Sari, B. and Siano, P. (2023). Nonlinear Optimal Control for a Gas Compressor Actuated by a Five-Phase Induction Motor. *Power Electronics and Drives*, 8(1), pp. 196–218. doi: 10.2478/pead-2023-0014.

Saad, K., Abdellah, K., Ahmed, H. and Iqbal, A. (2019). Investigation on SVM-Backstepping Sensorless Control of Five-Phase Open-End Winding Induction Motor Based on Model Reference Adaptive System and Parameter Estimation. *Engineering Science and Technology, an International Journal*, 22(4), pp. 1013–1026. doi: 10.1016/j.jestch.2019.02.008.

Sahraoui, K., Kouzi, K. and Ameur, A. (2017). Optimization of MRAS based Speed Estimation for Speed Sensorless Control of DSIM via Genetic Algorithm. *Electrotehnica, Electronica. Automatica*, 65(3), pp. 156–162.

Salem, A. and Narimani, M. (2019). A Review on Multiphase Drives for Automotive Traction Applications. *IEEE Transactions on Transportation Electrification*, 5(4), pp. 1329–1348. doi: 10.1109/TTE.2019.2956355.

Schauder, C. (1989). Adaptive speed identification for vector control of induction motors without rotational transducers. In: *Proceedings of the Conference Record of the IEEE Industry Applications Society Annual Meeting*. San Diego, CA, USA, 01-05 October 1989. doi: 10.1109/IAS.1989.96696.

Slunjski, M., Dordevic, O., Jones, M. and Levi, E. (2020). Symmetrical/Asymmetrical Winding Reconfiguration in Multiphase Machines. *IEEE Access*, 8, pp. 12835–12844. doi: 10.1109/ACCESS.2020.2965652.

Stando, D. and Kazmierkowski, M. P. (2020). Simple Technique of Initial Speed Identification for Speed-Sensorless Predictive Controlled Induction Motor Drive. *Power Electronics and Drives*, 5(1), pp. 189–198. doi: 10.2478/pead-2020-0014.

Szczepanski, R., Tarczewski, T. and Grzesiak, L. M. (2019). Adaptive State Feedback Speed Controller for PMSM Based on Artificial Bee Colony Algorithm. *Applied Soft Computing*, 83, p. 105644. doi: 10.1016/j.asoc.2019.105644.

Wang, F., Zhang, Z., Mei, X., Rodríguez, J. and Kennel, R. (2018). Advanced Control Strategies of Induction Machine: Field Oriented Control, Direct Torque Control and Model Predictive Control. *Energies*, 11(1), p. 120. doi: 10.3390/en11010120.

Yang, G., Yang, J., Li, S., Wang, Y., Hussain, H., Yan, L. and Deng, R. (2021). Overmodulation Strategy

for Seven-Phase Induction Motors with Optimum Harmonic Voltage Injection based on Sequential Optimization Scheme. *IEEE Transactions on Power Electronics*, 36(12), pp. 14039–14050. doi: 10.1109/TPEL.2021.3083974.

Yousfi, L., Aoun, S. and Sedraoui, M. (2022). Speed Sensorless Vector Control of Doubly Fed Induction Machine using Fuzzy Logic Control Equipped with Luenberger Observer. *International Journal of Dynamics and Control*, 10(6), pp. 1876–1888. doi: 10.1007/s40435-022-00946-0.

Zellouma, D., Bekakra, Y. and Benbouhenni, H. (2023). Field-Oriented Control based on Parallel Proportional–Integral Controllers of Induction Motor Drive. *Energy Reports*, 9, pp. 4846–4860. doi: 10.1016/j.egyr.2023.04.008.

Zhang, J., Jin, Z., Zhao, Y., Tang, Y., Liu, F., Lu, Y. and Liu, P. (2020). Design and Implementation of Novel Fractional-Order Controllers for Stabilized Platforms. *IEEE Access*, 8, pp. 93133–93144. doi: 10.1109/ACCESS.2020.2994105.

Zhou, M., Cheng, S., Feng, Y., Xu, W., Wang, L., and Cai, W. (2021). Full-order terminal sliding-mode-based sensorless control of induction motor with gain adaptation. *IEEE Journal of Emerging and Selected Topics in Power Electronics*, *10*(2), 1978-1991. doi: 10.1109/JESTPE.2021.3081863.